




Optical and dielectric studies of CdI₂-doped silver borotellurate glass system

Puli Nageswar Rao^{1,*} , M. Chandra Shekhar Reddy², A. Prabhakar Reddy³, E. Ramesh Kumar⁴, and B. Appa Rao⁴

¹Department of S&H, St. Martin's Engineering College, Secunderabad 500100, India

²Department of S&H, CMR College of Engineering & Technology, Secunderabad, India

³Department of H&S, Sreyas Institute of Engineering & Technology, Hyderabad, India

⁴Department of Physics, Osmania University, Hyderabad 500 007, India

Received: 10 July 2020

Accepted: 9 November 2020

Published online:
24 November 2020

© Springer Science+Business
Media, LLC, part of Springer
Nature 2020

ABSTRACT

This paper treaty with the preparation, characterization, and Optical and Dielectric studies of $x\text{CdI}_2-(100-x)[0.444\text{Ag}_2\text{SO}_4-0.555(0.4\text{TeO}_2-0.6\text{B}_2\text{O}_3)]$ glass system, where x is the wt% of CdI₂ varying from 0 to 25 with step 5. These systems were prepared by melt quenching method and characterized by Differential scanning calorimeter (DSC), X-ray diffraction (XRD), and Fourier transforms infrared (FTIR) spectra. Physical parameters such as the density of materials, molar volume, average molecular weight, refractive index, oxygen mole present, polarizability, field strength, and Cd and Ag ions concentration were calculated. Based on optical absorption results, direct band gap E_g was premeditated by comparing Tauc's plots and the ASF method. From these optical absorption results, Urbach energy (E_u) also calculated. Second-order deformation potential and free energy of the system have been resolved by expending relation between E_u and E_g . Variation of these factors by changing the CdI₂ composition is deliberated in detail. Refractive index, dielectric constant at optical and electrical frequencies have been discussed in detail.

1 Introduction

In recent years, silver-doped borotellurite glass and glass–ceramics have abundant attention because of its valuable high value of ionic, dielectric, and optical properties. These types of materials are of technical and industrial interest in view of their applications including fuel cells, optical switches, biosensors, primary batteries, etc. [1–4]. So many studies

evidenced that the glassy nature of the substances exhibits valuable optical properties and higher dielectric properties than their corresponding crystalline equivalents. The optical, structural, and electrical properties depend on the content and glass former nature, modifier oxide, and also dopant salt compositions [1–4]. Pure borotellurite glasses are concocted of a random network of boroxyl structural units through boron in threefold co-ordination (BO₃)

Address correspondence to E-mail: nageswarapuli@gmail.com

and arbitrary network of telluride units through tellurium in twofold co-ordination (TeO_2). The accumulation of dopant salt and modifier leads the creation of BO_4 , TeO_3 , TeO_4 clusters and formation of non-bridging oxygen. The rise of formation of non-bridging oxygen benefits to open the network arrangement and the rise of dielectric constant and Urbach energy values [3–7]. Rigorous studies on the structural, optical, and dielectric properties of silver doped with glass formers B_2O_3 and TeO_2 , and glass modifier Ag_2SO_4 have been most familiar in recent studies [2, 3, 7, 8]. Ionic conductivity studies of the present system are published in our previous journal [2]. In this current study, $x\text{CdI}_2-(100-x)[m\text{Ag}_2\text{SO}_4-f(0.4\text{TeO}_2-0.6\text{B}_2\text{O}_3)]$ system was used for dielectric and optical measurements. Here, m and f are the Wt% of glass modifier such as Ag_2SO_4 and Wt% glass formers such as $\text{B}_2\text{O}_3 + \text{TeO}_2$, and their ($m = 0.444$, $f = 0.555$) ratio ($m/f = 0.8$) was kept constant, where x is the Wt% of CdI_2 changing from 0 to 25 with step 5. The objective of the present work is to throw a certain focus on the dielectric properties and optical properties of the CdI_2 -doped glass system.

2 Experimental

Glass system $x\text{CdI}_2-(100-x)[0.444\text{Ag}_2\text{SO}_4-0.555(0.4\text{TeO}_2-0.6\text{B}_2\text{O}_3)]$ was prepared by the melt quenching method, and this preparation method was also published in our previous journal [2]. Pure AR grade raw materials CdI_2 , TeO_2 , H_3BO_3 , and Ag_2SO_4 were mixed thoroughly in an agate mortar, and the batch was heated in the temperature range 730–770 °C for about 30 min. In this temperature range, viscous and uniform melt was formed. Thin and smooth specimens were obtained by pouring the viscous, uniform melt on a rectangular or square brass mold which is placed at 27 °C and hard pressed with one more smooth plate to get thin CBT samples. Based on the dopant salt composition, prepared samples were labeled as CBT 0, CBT 5, CBT 10, CBT 15, CBT 20, and CBT 25, and its composition is listed in Table 1.

The surface of the samples was polished with sandpaper and velvet cloth to obtain a thin and smooth surface. Using the PANalytical Philips X'pert pro Diffractometer with $\text{CuK}\alpha$ radiation ($\lambda = 1.54056 \text{ \AA}$) and differential scanning calorimeter (DSC) on DSC Q20, the nature of the CBT samples

was investigated. Using the BRUKER TENSOR-27 spectrometer, Fourier transform infrared (FTIR) spectra of the CBT samples were recorded in the range of 250–4000 cm^{-1} wavenumber. By using the Wayne Kerr precision component analyzer, the impedance measurements were investigated. In this experiment, the silver-coated sample is sandwiched between the two electrodes, and the thin silver wires from the two discs are connected to the LCR meter and measure the imaginary and real parts of impedance (Z), and phase angle (θ). The optical absorption measurements were recorded using a recording spectrometer of kind Labindia analytical UV 3092 UV-VIS spectrometer. The optical absorption spectra were taken from the transmittance spectra of the CBT samples which measure using the sample-in sample-out method [9]. The density (ρ) of CBT samples at room temperature was measured by the standard Archimedes principle using a more sensitive digital balance and *O*-xylene used as a buoyant. The following well-known formula was used to calculate the density of CBT samples:

$$\rho = \frac{W_a}{W_a - W_x} \rho', \quad (1)$$

where W_x and W_a are the weight measurement of the CBT sample in *O*-xylene and the weight of the CBT sample in air and ρ' is *O*-xylene density at ambient temperature. Using a numerical balance (Essae vibra HT digital balance), all the measurements were made, and to get accurate values, the experiments were performed 3 or 4 times. The accuracy in the density measurements is $\pm 0.0005 \text{ g cm}^{-3}$, and the percentage of error in the measurements of density was $\pm 0.001 \text{ g cm}^{-3}$.

The molar volume (V_m) of the CBT Samples was calculated, and it is defined as the ratio of average molecular weight (\bar{M}) of the CBT samples and density (ρ) of the CBT samples, it also represented in the following equation:

$$V_m (\text{cc/mole}) = \bar{M}/\rho, \quad (2)$$

where $\bar{M} = \sum n_i A_i$. Here A_i and n_i denote the molecular weight of i th component and molar concentrations of the i th component.

Dopant ion concentration (N_i), interionic distance r_i (\AA), Polaron radius r_p , oxygen packing density O , and field strength F_i of the CBT samples were calculated by using the following equations:

Table 1 Composition of prepared samples

Sample code	X	Composition: $x \text{ CdI}_2 - (100 - x)[0.444\text{Ag}_2\text{SO}_4 - 0.555(0.4\text{TeO}_2 - 0.6\text{B}_2\text{O}_3)]$
CBT 0	0	$[0.444\text{Ag}_2\text{SO}_4 - 0.555(0.4\text{TeO}_2 - 0.6\text{B}_2\text{O}_3)]$
CBT 05	05	$05 \text{ CdI}_2 - 95[0.444 \text{ Ag}_2\text{SO}_4 - 0.555(0.4\text{TeO}_2 - 0.6\text{B}_2\text{O}_3)]$
CBT 10	10	$10 \text{ CdI}_2 - 90[0.444 \text{ Ag}_2\text{SO}_4 - 0.555(0.4\text{TeO}_2 - 0.6\text{B}_2\text{O}_3)]$
CBT 15	15	$15 \text{ CdI}_2 - 85[0.444 \text{ Ag}_2\text{SO}_4 - 0.555(0.4\text{TeO}_2 - 0.6\text{B}_2\text{O}_3)]$
CBT 20	20	$20 \text{ CdI}_2 - 80[0.444 \text{ Ag}_2\text{SO}_4 - 0.555(0.4\text{TeO}_2 - 0.6\text{B}_2\text{O}_3)]$
CBT 25	25	$25 \text{ CdI}_2 - 75[0.444 \text{ Ag}_2\text{SO}_4 - 0.555(0.4\text{TeO}_2 - 0.6\text{B}_2\text{O}_3)]$

$$N_i \text{ (ions /cm}^3\text{)} = \frac{\rho F_w N_A}{M_w}, \quad (3)$$

$$r_i = \left[\frac{1}{N_i} \right]^{1/3}, \quad (4)$$

$$r_p(\text{\AA}) = \frac{1}{2} \left[\frac{\pi}{6N_i} \right]^{1/3}, \quad (5)$$

$$O = (\rho/M) \times n, \quad (6)$$

$$F_i = \frac{Z}{r_p^2}, \quad (7)$$

where F_w , ρ , M_w , N_A , n , and Z are weight fraction of dopant salt, the density of the glass sample, the average molecular weight of dopant salt and Avogadro number, number of Oxygen atoms per formula unit, and oxidation number, respectively. The physical properties of the CBT samples have been calculated by using following equations:

Dielectric measurements were made with the Wayne Kerr LCR-6440B impedance analyzer in the frequency range of 20 Hz–3 MHz. Well-polished and silver-coated CBT samples were used for impedance analysis. In the samples, if the applied electric field varies with time, then the induced charge on the sample is represented as follows:

$$Q = \varepsilon^* V_0 \exp(j\omega t), \quad (8)$$

where ε^* is the complex value of dielectric constant and it can be written as

$$\varepsilon^*(\omega) = \varepsilon'(\omega) + i\varepsilon''(\omega), \quad (9)$$

where ε' is the real component and ε'' is the imaginary component, and it represents the storage of the energy and loss of the energy for the duration of each cycle of the electric field, respectively.

The real component ε' and imaginary component ε'' of complex dielectric constant can be represented as follows:

$$\varepsilon' = \frac{t}{A\omega\varepsilon_0} \left[\frac{Z''}{Z'^2 + Z''^2} \right], \quad (10)$$

$$\varepsilon'' = \frac{t}{A\omega\varepsilon_0} \left[\frac{Z'}{Z'^2 + Z''^2} \right]. \quad (11)$$

In the present study, real as well as imaginary parts of the complex dielectric permittivity were calculated from the measured impedance data by using the above equations.

3 Results and discussion

3.1 X-ray diffraction (XRD) differential scanning calorimeter (DSC) and Fourier transforms infrared (FTIR) spectra

The room-temperature XRD, DSC, and FTIR patterns of all CBT samples are published in our previous paper, and XRD and FTIR patterns are also shown in Figs. 1a and 2.

From XRD patterns, the absence of sharp peaks and DSC thermograms indicate the amorphous (glass) nature of the prepared CBT samples from CBT 0 to CBT 20, and these results are published in our previous journal [2]. Further, increasing the CdI_2 concentration amorphous nature of the CBT samples decreases; this indicates that in the amorphous background, partial crystallization takes pace, which is also observed in DSC studies [2]. FTIR spectra of CBT samples are shown in Fig. 2; in the present spectra, there are two fundamental modes TeO_4 trigonal bipyramids (tbp) bands $\nu_{\text{ax}}^{\text{as}}$, $\nu_{\text{eq}}^{\text{as}}$, and two TeO_3 trigonal pyramids (tp) ν^{d} and ν^{s} ; TeO_3 fundamental modes of vibration are presented at 672 cm^{-1} , 718 cm^{-1} , 748 cm^{-1} , and 653 cm^{-1} , respectively [1, 2, 10].

The spectral bands due to B–O vibrations in BO_3 exhibited in the range of $1200\text{--}1600 \text{ cm}^{-1}$ and BO_4

Fig. 1 **a** XRD patterns of CBT samples at different compositions. **b** Relation between density and molar volume of CBT samples

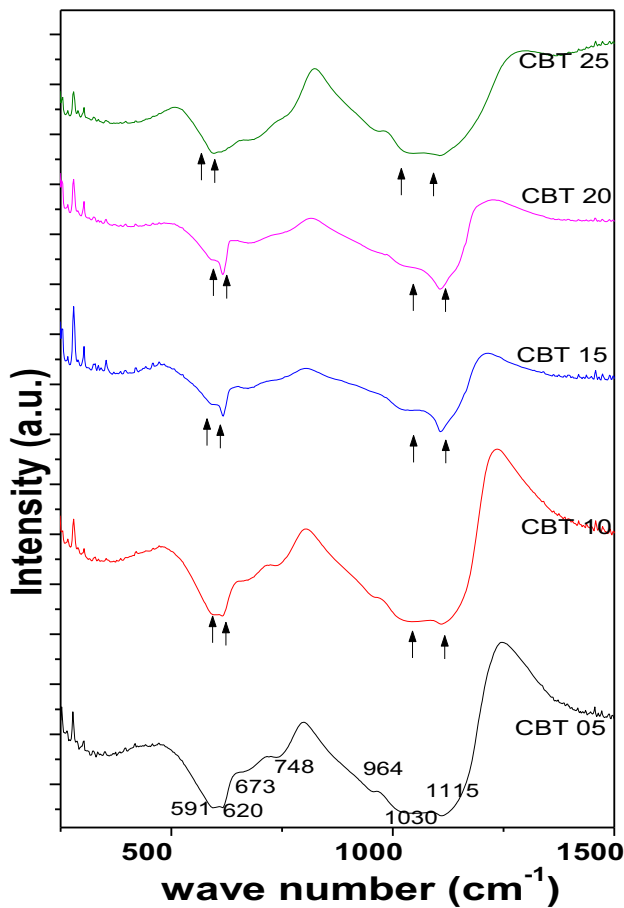
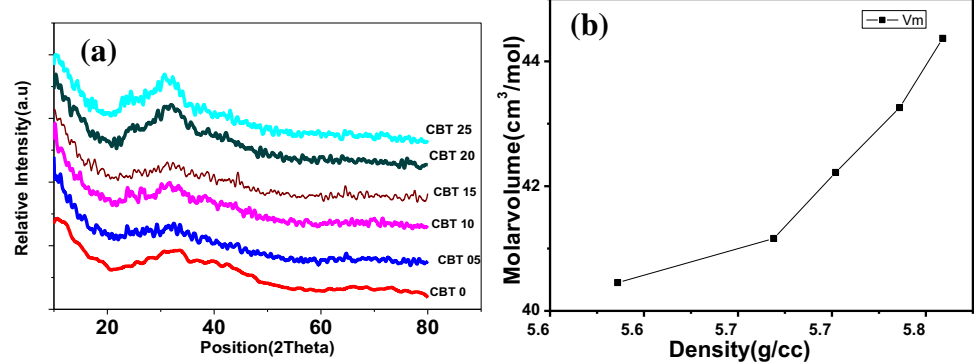


Fig. 2 FTIR spectra of prepared CBT samples

structural units in the range of 1370–1050 cm^{-1} and B–O–B linkages is presented at $\sim 720 \text{ cm}^{-1}$ [2, 10–16]. The bands ν_3 and ν_4 vibrations of sulfate (SO_4^{2-}) groups, S=O stretching bands and SO_3^{2-} groups shown in Fig. 2, and discussed in our previous publication [2]. The intensity of IR bands ~ 620 and $\sim 1115 \text{ cm}^{-1}$ rises with enhancing the CdI_2 composition as well as with increasing CdI_2 concentration intensity of IR bands exhibited at near

600 cm^{-1} and 1000 cm^{-1} are decreased, and it can be associated with additional creation of SO_3^{2-} and TeO_3 units. This leads to the increment of disorder CBT glass system with increasing CdI_2 concentration [2, 17]. The addition of CdI_2 dopant salt plays a key role to enhance the formation of $[\text{TeO}_3]^{2-}$, $[\text{BO}_3]^-$, and $[\text{SO}_3]^{2-}$ at the expense of $[\text{TeO}_4]^{2-}$, $[\text{BO}_4]^-$, and $[\text{SO}_4]^{2-}$ groups, respectively. This may lead to an increase in NBO's, non-bridging sulfates, and amorphous nature of CBT samples. These structural changes help to enhance the mobility of Ag^+ ions. It leads to a decrease in the activation energy, which is responsible for the enhancement of dielectric and optical properties of CBT samples [2].

3.2 Physical parameters

The physical parameters of CBT samples have been calculated using Eqs. 1–7 and listed in Table 2. Average molecular weight has been found to increase from 225.971 to 255.497 g/mol with increasing CdI_2 composition; also density (from 5.586 to 5.759 g/cc), molar volume (from 40.452 to 44.368 cm^3/mole), molar refraction (from 25.06694 to 39.1948), polarizability (from $9.941 \times 10^{-24} \text{ cm}^3$ to $15.543 \times 10^{-24} \text{ cm}^3$), Cd^{2+} ion concentration (from $1.489 \times 10^{21}/\text{cc}$ to $6.787 \times 10^{21}/\text{cc}$), field strength of Cd ions (from $0.803 \times 10^{15}/\text{\AA}^2$ to $2.208 \times 10^{15}/\text{\AA}^2$), interionic distance between Ag ions (from 4.301 to 4.799 \AA), refractive index (from 2.4265 to 4.8713), and Polaron radius of Ag ions (from 1.733 to 1.934 \AA) have been found to increase with increasing CdI_2 composition. Oxygen mol% (from 2.956 to 2.333), Oxygen packing density (from 73.062 to 52.589 g atom/L), interionic distance between Cd ions (from 8.757 to 5.281 \AA), Ag^+ concentration (from $12.567 \times 10^{21}/\text{cc}$ to $9.049 \times 10^{21}/\text{cc}$), field strength of Ag ions (from $3.330 \times 10^{15}/\text{\AA}^2$ to $2.674 \times 10^{15}/\text{\AA}^2$)

Table 2 Physical parameters of all CBT samples

	Physical parameter	Glass				
		CBT 05	CBT 10	CBT 15	CBT 20	CBT 25
1	Average M_w (g/mol)	225.971	233.352	240.734	248.116	255.497
2	Density, ρ (g/cc) (± 0.001)	5.586	5.669	5.702	5.736	5.759
3	Refractive index, n (± 0.001)	2.4265	2.555	2.895	4.652	4.8713
4	Molar volume, V_m (M_w/ρ) (± 0.01)	40.452	41.161	42.219	43.258	44.368
5	Molar refraction, R_M (± 0.001)	25.067	26.681	29.805	39.687	39.195
6	Polarizability, α_e ($\times 10^{-24}$ cm ³) (± 0.001)	9.941	10.581	11.820	15.739	15.543
7	Oxygen mol %, O (± 0.001)	2.956	2.800	2.644	2.489	2.333
8	Oxygen packing density (g atom/L) (± 0.001)	73.062	68.024	62.636	57.535	52.589
9	Cd ²⁺ ion concentration, N_i ($\times 10^{21}$ /cc) (± 0.001)	1.489	2.926	4.280	5.569	6.787
10	Ag ⁺ concentration, N_i ($\times 10^{21}$ /cc) (± 0.001)	12.567	11.692	10.781	9.900	9.049
11	Interionic distance, r_i (Å) (± 0.001) (Cd)	8.757	6.991	6.159	5.641	5.281
12	Polaran radius, r_p (Å) (± 0.001) (Cd)	3.529	2.817	2.482	2.273	2.128
13	Interionic distance, r_i (Å) (± 0.001) (Ag ₂ SO ₄)	4.301	4.404	4.527	4.657	4.799
14	Polaran radius, r_p (Å) (± 0.001) (Ag ₂ SO ₄)	1.733	1.775	1.824	1.877	1.934
15	Field strength of Cd ²⁺ ($10^{15}/\text{Å}^2$)	0.803	1.260	1.623	1.935	2.208
16	Field strength Ag ⁺ ($10^{15}/\text{Å}^2$)	3.330	3.175	3.005	2.840	2.674
17	Metallization factor	0.38033	0.35178	0.28905	0.12689	0.1166

and Polaran radius Cd ions (from 3.529 to 2.128 Å) and metallization factor are found (from 0.38033 to 0.1166) to decrease with increase in CdI₂ composition. The molar volume of the samples depends on the density of the samples, and the relationship between density and molar volume is shown in Fig. 1b. From the data, it is clear that the density of samples enhances with the addition of CdI₂ concentration because the relative molecular mass of CdI₂ is greater than that of Ag₂SO₄ and glass formers (TeO₂ and B₂O₃). But increasing in CdI₂ content enhances the number of Ag⁺ ions in the shallow iodide potential and at the same time decreases the number of Ag⁺ ions in the sulfate anion potentials. When such potentials are associated for an extensive period, they form a favorable path for ion transport known as diffusion path. Thus, the increase in CdI₂ concentration creates more and more diffusion paths by increasing the dielectric and optical properties [2].

3.3 Optical properties

To find out the electronic structure of glasses, optical absorption spectra are one of the best useful tools [18]. The coefficient of optical absorption (α) has been determined at below or near the edge of each curve and also using well-known Eq. (12):

$$\alpha = \frac{1}{t} \ln \left(\frac{I_0}{I_T} \right), \quad (12)$$

where I_T and I_0 are intensities of the transmitted and incident beams, respectively, and t is the thickness of each sample. Cutoff wavelength for the base glass system is about 435 nm. After adding the dopant salt to the base glass system, initially cutoff wavelength decreased, and on increasing dopant salt concentration, it is increased compared to the base glass system, which is shown in Fig. 3. The relation between the coefficient of optical absorption (α) and the optical band gap (E_g) is stated by Eq. (13), and optical band gap of the CBT samples was measured from this equation [18, 19]

$$(\alpha h\nu)^n = B^{1/n} (h\nu - E_g), \quad (13)$$

where B and n denote band tailing parameter (is a constant) and the type of optical transition, respectively, $n = 1/2$ represents allowed direct, 2 represents allowed indirect, $1/3$ represents forbidden direct, and 3 represents forbidden indirect transitions and ν is the energy of incident photons. In direct allowed transitions, the photons can assist the more electrons to jump from lower energy valence band to higher energy conduction band. Total energy and momentum of the photon and as well as electron system are

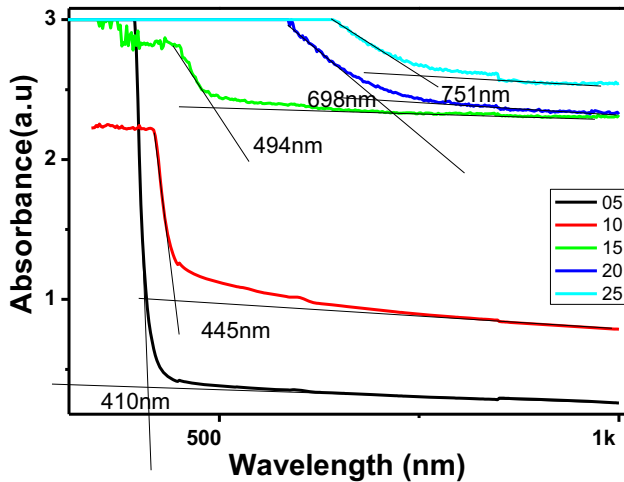


Fig. 3 Optical absorption spectra of CdI₂-doped samples

conserved in the transition process [1, 17, 20, 21]. But, in the case of indirect transitions process to conserve momentum, the absorption or emission of a phonon involved, and the lower energy level of the conduction band and the higher energy level of the valence band take place at different wave vectors in the Brillion zone [1, 20–22]. The E_g value in the CBT glass system is resolute from the locus of the absorption edge, and it gives evidence about the width of the localized positions [22]. The E_g value of the system also gives facts about the nature and chemical bonds of the CBT glass structure [22].

Tauc plots for all transitions have been plotted, such as forbidden direct $((\alpha hv)^{1/3}$ vs hv), forbidden indirect $((\alpha hv)^3$ vs hv), direct allowed $((\alpha hv)^{1/2}$ vs hv), and indirect allowed $((\alpha hv)^2$ vs hv), as shown in Fig. 4. By extrapolating the linear region of above curves to the x -axis, optical band-gap energy E_g values were calculated, i.e., $(\alpha hv)^{1/2} = 0$ for allowed direct, $(\alpha hv)^2 = 0$ for indirect, $(\alpha hv)^{1/3} = 0$ for forbidden direct, and $(\alpha hv)^3$ for forbidden indirect transitions. The values of E_g are shown in Table 3, and these values are found to rise with CdI₂ concentration. Energy gap (E_g) values may not be resolute accurately by alone fatiguing optical absorbance measurements. To find out optical band-gap energy more accurately, Souri et al. and Alarcon et al. [17, 23] suggested that a method is called optical absorption spectrum fitting (ASF), and Eq. (13) can be modified as Eq. (14) as follows:

$$\alpha(\lambda) = \text{const}(hc)^{n-1} \lambda \left(\frac{1}{\lambda} - \frac{1}{\lambda_g} \right)^n, \tag{14}$$

where h is Plank’s constant, c is the light speed, and

λ_g wavelength consistent to the optical gap. Integrating Beer–Lambert’s law into Eq. (14), the absorbance $\alpha(\lambda)$ can be expressed as follows:

$$\alpha(\lambda) = D_1 \lambda (1/\lambda - 1/\lambda_g)^n + D_2, \tag{15}$$

where $D_1 = \text{const} (hc)^{n-1} d/2.30$, D_2 is another constant, and it gives the information about reflection of incident light lost. Assuming that the sum of fraction dispersed or reflected light is small. Using Eq. (14), without the need for thickness (t), the E_g value can be calculated from the ASF method of the CBT glass samples. In Fig. 5, undeviating region of $(A/\lambda)^{1/n}$ versus $(1/\lambda)$ plot extrapolating to $(A/\lambda)^{1/n}$ is zero to obtain optical band-gap (E_g^{asf}) value. The finest fit is detected for ‘ n ’ equal to ‘2’, and E_g^{asf} value is intended from the parameter λ_g using the expression:

$$E_g^{\text{asf}} = \frac{1239.83}{\lambda_g}. \tag{16}$$

The calculated E_g^{asf} obtained from $(A/\lambda)^{1/n}$ versus $(1/\lambda)$ plot values are similar to E_g^{opt} obtained from the Tauc plots of $(\alpha hv)^{1/2}$ versus (hv) , and these values are listed in Table 3. From the above results, we can conclude that band gap is a direct band gap, and transitions are direct for all CBT samples [20, 22].

The activation energy of the CBT system has been calculated from the dc conductivity studies, and values are listed in Table 3 and published in our previous paper [2]. This value decreases with increasing the composition; similarly the optical band gap also decreases with increasing the composition. The optical band gap depends on the composition of the material, NBOs and NBSs but activation energy depends on mobility of the Ag ions in the glass matrix and availability of Ag ions. In the present system, activation energy value is smaller than the optical band-gap value.

All CBT samples follow the Urbach law shown in Eq. (17) [21]:

$$\alpha(\nu) = (\text{const.}) e^{\frac{h\nu}{E_u}}, \tag{17}$$

where E_u denotes the Urbach energy. Urbach energy value is interpreted as the width of the tail of the localized energy states in the optical band gap. The above relation can be expressed following Eq. (18):

$$\ln \alpha(\nu) = (h\nu/E_u) - \text{const.} \tag{18}$$

Figure 5a shows that the plots of $(\ln(\alpha))$ vs $(h\nu)$ are named as Urbach plots. From the reciprocal of slopes

Fig. 4 Tauc plots of **a** direct allowed, **b** indirect allowed, **c** forbidden direct, and **d** forbidden indirect transitions of all CBT samples

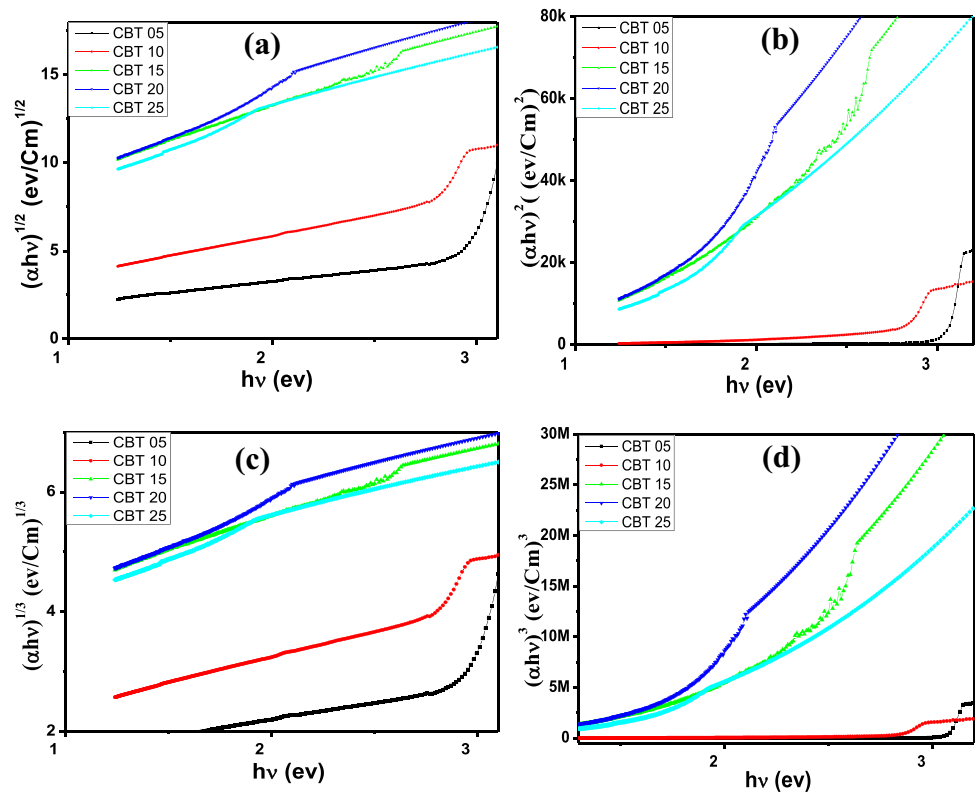


Table 3 Optical parameters of all CBT samples

Sample	E_g^{opt}	E_g^{opt}	E_g^{opt} (ev)	E_g^{opt} (ev)	E_g^{asf}	E_u	E_g^{elc} (ev)	R.I	(nm)	Dielectric constant
	(ev)	(ev)								
CBT 05	2.893	3.064	2.826	3.08	2.839	0.138	0.403	2.426	410	5.885
CBT 10	2.475	2.762	2.635	2.829	2.343	0.263	0.379	2.555	445	6.528
CBT 15	1.671	2.312	1.455	2.504	1.773	0.889	0.340	2.895	494	8.381
CBT 20	0.322	1.670	1.241	1.58	0.323	1.833	0.325	4.652	698	21.641
CBT 25	0.272	1.383	1.194	1.541	0.277	2.116	0.368	4.871	751	23.727

of linear regions of $(\ln(x))$ vs (hv) plots, E_u was calculated and the values are listed in Table 3.

In the CBT glass system, structural disorder plays an important role, and non-bridging oxygen (NBO) atoms and dangling bonds are the main cause of these structural disorders [22]. From the E_u values, it was observed that with an increase in CdI_2 content, there is an increase in E_u value. This is due to an increase of NBOs with intensification in the CdI_2 , and results were reinforced by FTIR results as shown in Fig. 2.

The relation between E_g and E_u is shown in Fig. 6b, E_g values decrease with increasing E_u . Following well-known equation states that numerical relationship between E_g and E_u [20, 21]:

$$E_g = E_f - GE_u, \quad (19)$$

where E_f stands for the free energy of the CBT system depends on local co-ordination and it is also a constant, and the value for the CBT system is 2.922 eV. G is constant, its value for the CBT system is 1.331 and it also proportional relation with second-order distortion potential value. G and E_f values of the CBT

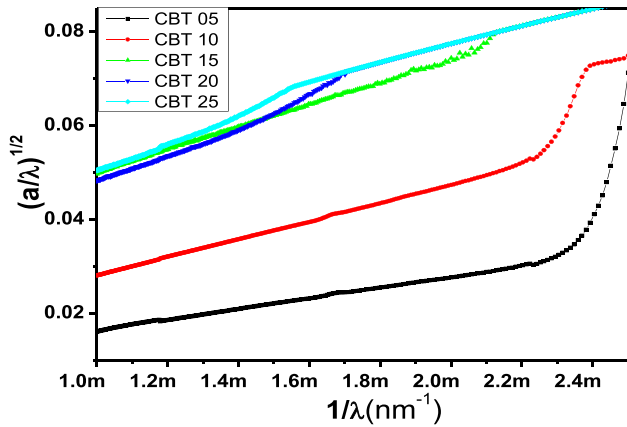


Fig. 5 ASF method to find energy gap of CBT samples

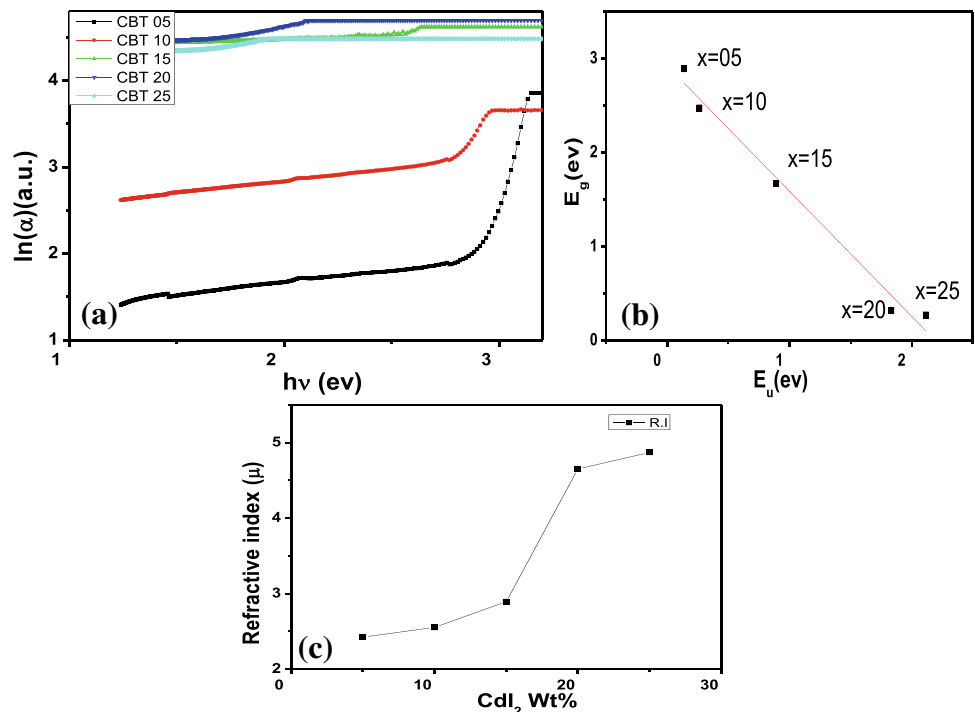
glass system were achieved from the slope and intercept of the plot in Fig. 6b.

From optical band-gap energy, the refractive index (μ) of the CBT glass system was calculated using the following equation proposed by Sakka and Dimitrov [22]:

$$\frac{\mu^2 - 1}{\mu^2 + 2} = 1 - \sqrt{\frac{E_g}{20}}, \tag{20}$$

where μ values of the CBT samples rise with CdI₂ composition shown in Fig. 6c, the values are listed in Table 3, and the range of values from 2.426 to 4.871.

Fig. 6 a The Urbach plots of all CBT samples. b The variations of E_g with E_u . c The variations of refractive index with composition



These high refractive index materials are used in wave guide applications.

The refractive index (μ) of material is linked to the dielectric constant (ϵ) via a following simple relation. Dielectric constant (ϵ) values of CBT systems of samples at optical frequencies are calculated by using Eq. 21, and these values are listed in Table 3. Dielectric constant at optical frequencies of the CBT samples increases from 5.885 to 23.727 with increasing CdI₂ composition:

$$\epsilon = \mu^2. \tag{21}$$

3.4 Frequency-dependent refractive index and dielectric constant

Frequency-dependent refractive index μ can be calculated from the following modified Fresnel equation [1, 24–27]:

$$\mu = \frac{1 + R + \sqrt{4R - (1 - R^2k^2)}}{1 - R}, \tag{22}$$

where k is the extinction coefficient or imaginary part of refractive index, and R is reflection. The spectral dependence of the k' is given by Eq. 23 [1, 25]:

$$k = \frac{\alpha\lambda}{4\pi}. \quad (23)$$

The values of refractive index (μ) and extinction coefficient (k) has further been used to determine real (ϵ') part and imaginary (ϵ'') part of dielectric constant, and relations are shown in the following equations [1, 25]:

$$\epsilon' = \mu^2 - k^2, \quad (24)$$

$$\epsilon'' = 2\mu k. \quad (25)$$

Figure 7 shows the real and imaginary parts of dielectric constant ϵ' and ϵ'' dependence on photon energy. It can be observed that ϵ' and ϵ'' increase with CdI_2 composition up to 20 wt%, and after that they decrease. Figure 7 shows that the peak position ϵ' curve shifts to lower energy side with increasing CdI_2 , this indicates that the decrease in the optical band gap with increasing CdI_2 wt%; it also observed that sudden increase in the imaginary part of dielectric constant ϵ'' specifies that the position of an absorption edge changes with the composition [1, 27].

The optical band gap E_g also can be obtained by extrapolating ϵ' to zero, and these values are in good agreement with the values estimated from direct band-gap values [1, 25–27]. In the present system at lower compositions, we can obtain E_g value for getting the E_g value at higher compositions graph should extend to lower frequency values.

3.5 Dielectric permittivity

Dielectric permittivity is a characteristic of short-range electrical conduction of material under the effect of an applied electric field [28]. When a field is applied to prepared CBT samples, the applied field will transfer the charges in the interior of the CBT

glass material and affect the pileup of charge at the interface, and creating dipoles with a moment $\mu = Q\delta$, where Q is the charge and δ is the average separation space between the charges and $Q = CV$, where C is the capacitance of the materials and is given by $C = C_o\epsilon/\epsilon_o$, where C_o is the capacitance of free space and is given by $C_o = \epsilon_o A/t$, where ϵ_o is the permittivity of vacuum or free space, t and A are the thickness of the CBT samples and area of cross section of the material, respectively.

The AC response of the CBT system of samples has also been studied by calculating the dielectric constants. Figure 8 shows the real (ϵ') part and imaginary (ϵ'') part of the dielectric constant as a function of $\log(\text{frequency})$ of prepared CBT samples.

Figure 8 and b shows the real (ϵ') part and imaginary (ϵ'') part of the dielectric constant vs $\log(f)$ of different compositions of CdI_2 at room temperature, respectively. With increasing the CdI_2 compositions from 5 to 20 wt%, both the real and the imaginary parts of dielectric constant increase after that they decrease, particularly at lower frequencies. As the CdI_2 composition increases, charge carriers increases, typically connected with the polarization impacts the hopping of long-range charge carriers related to the constant glass matrix. As can be seen from the figures, ϵ' and ϵ'' decrease rapidly at low frequencies with increasing frequency and at the higher frequency side, the decrease is very less, all most constant. It might be due to space charge polarization (interfacial effects). With increasing the frequency, the polarizability due to orientational and ionic sources decreases, and finally polarizability vanishes due to inertia of the ions [7, 8]. Figure 9 shows that the rise in dielectric constant with an enhancement of temperature is typically connected with a reduction in bond energies. There are two effects on dipolar

Fig. 7 Variation of ϵ' and ϵ'' with optical energy of CBT samples

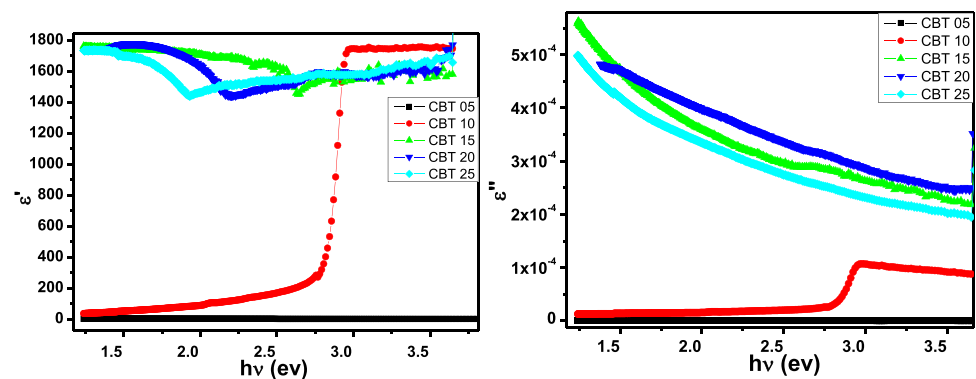
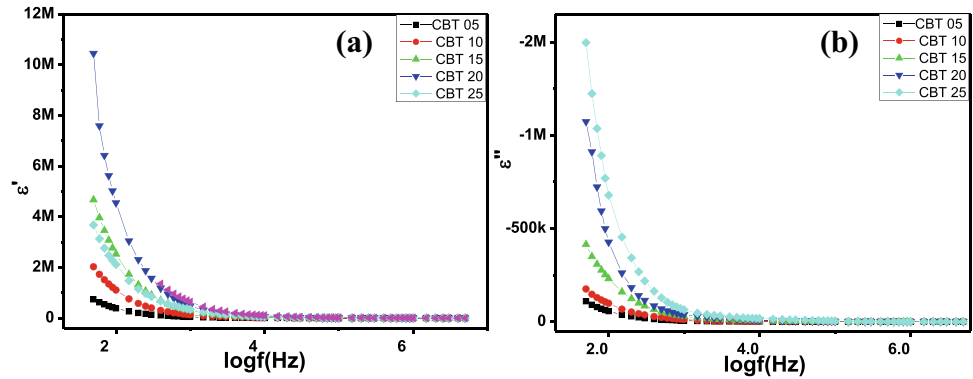


Fig. 8 Variation of ϵ' and ϵ'' with frequency of CBT samples at room temperature



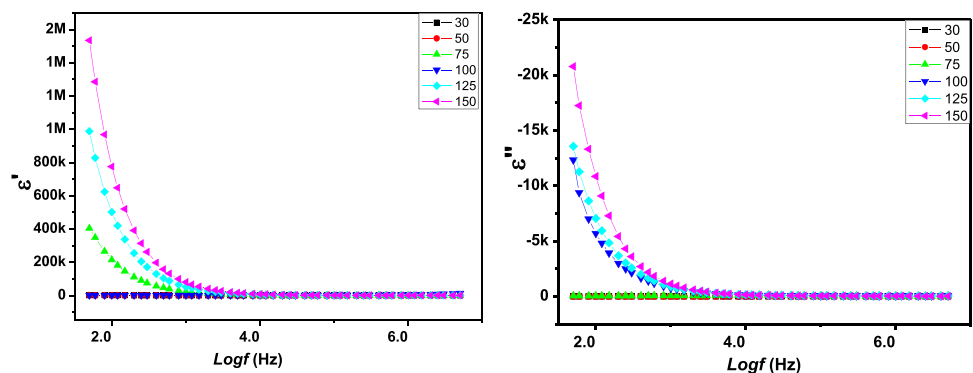
polarization that may take place with increasing the temperature: first one, the temperature may rise the thermal agitation and interrupts the orientational vibrations; the second one, the temperature may weaken the intermolecular forces and enhances the orientational vibrations [7, 8]. Furthermore, ϵ' increases more rapidly with temperature. The enhancement in dielectric constant (ϵ') with rising temperature is normally connected with a reduction in bond energies [7, 8]. It is, therefore, essential to examine the dielectric data using modulus representation, which quashes the dc polarization effect. Observing real and imaginary values of the graphs, the storage of the energy is more than the loss of energy during every cycle of the electric field.

4 Conclusions

The XRD study confirms that the glassy nature of CBT samples and glassy nature were found from 0 to 20 wt% of dopant salts concentration. The main physical parameters, density and molar volume, increase with increasing CdI₂ composition. FTIR results show that with increasing CdI₂ content, there is an additional creation of TeO₃, SO₃²⁻, and BO₃

units. Optical absorption spectra were recorded for all the samples of CBT systems at room temperature. Optical parameters such as optical band-gap energy and Urbach energy E_u were calculated for all CBT samples. Cutoff wavelength was observed to increase with increasing CdI₂ concentration. A good correlation was observed between the optical energy gaps calculated from the absorption spectrum fitting (ASF) method and Tauc's plots. From this, we can conclude that band gap is a direct band gap, and its transitions also direct for all CBT samples. From Urbach energy and FTIR results, the concentration of NBO's rises with enhancement of CdI₂ content. The values of E_f and G for the CBT glass system are 2.922 eV and 1.331, respectively. The high value of polarizability α_e (> 3) confirms the ionic nature of CBT glass samples. The refractive index increases with CdI₂ concentration and reaches a maximum value of 4.871. The dielectric constant value at optical frequencies of CBT glass samples increases with dopant salt concentration and ranges between 5.885 and 23.727. The real part and imaginary part of dielectric permittivity at optical and electrical frequencies increase with increasing of CdI₂ concentration. Optical and dielectric results show that the CBT samples have

Fig. 9 Variation of ϵ' and ϵ'' with frequency of CBT 05 samples at different temperature



ionic nature, good refractive index, and dielectric properties. These materials are suitable for waveguide applications and electrolyte material in solid-state batteries.

References

- P.N. Rao, E. Ramesh Kumar, Chandra Shekhar Reddy Madhureddy, A. Prabhakar Reddy, K. Krishnamurthy Goud, B. Appa Rao, Optical studies of AgI–Ag₂SO₄–TeO₂–B₂O₃ glass system. *Mater. Today Proc.* **5**(13, Part 1), 26329–26338 (2018)
- P.N. Rao, E. Ramesh Kumar, B. Appa Rao, Structural and transport studies of CdI₂-doped silver borotellurite fast ion-conducting system. *J. Solid State Electrochem.* **22**, 3863–3871 (2018). <https://doi.org/10.1007/s10008-018-4094-9>
- V. Sharma, S.P. Singh, G.S. Mudahar, K.S. Thind, Synthesis and optical characterization of silver doped sodium borate glasses. *New J. Glass Ceram.* **2**, 133–137 (2012). <https://doi.org/10.4236/njgc.2012.24019>
- M. Sharma, K.S. Thind, G. Sharma, V. Rajendran, K. Singh, A.V. Gayathri-Devi, S. Aravindan, Structural and acoustic investigations of calcium borate glasses. *Physica Status Solidi (A)* **203**(10), 2356–2364 (2006). <https://doi.org/10.1002/pssa.200622140>
- M. Pal, B. Roy, M. Pal, Structural characterization of borate glasses containing zinc and manganese oxides. *Int. J. Mod. Phys.* **2**, 1062 (2006). <https://doi.org/10.4236/jmp.2011.29129>
- P. Sharma, D.K. Kanchan, M. Pant, K.P. Singh, Conductivity studies in proton irradiated AgI–Ag₂O–V₂O₅–TeO₂ super-ionic glass system. *Mater. Sci. Appl.* **1**, 59–65 (2010). <http://doi.org/10.4236/msa.2010.12011>
- P.N. Rao, E. Ramesh Kumar, B. Appa Rao, Effect of quenching rate on electrical conductivity and glass formation of AgI–Ag₂SO₄–TeO₂–B₂O₃ system. *J. Mater. Sci. Mater. Electron.* **29**, 11247–11257 (2018). <https://doi.org/10.1007/s10854-018-9211-0>
- P.N. Rao, E. Ramesh Kumar, B. Appa Rao, Structural, electrical and transport number studies of AgI-doped silver borotellurite fast ion conducting glass system. *Ionic.* (2018). <https://doi.org/10.1007/s11581-018-2550-2>
- J. Ruiz-Fuertes, D. Errandonea, F.J. Manjón, D. Martínez-García, A. Segura, V.V. Ursaki, I.M. Tiginyanu, High-pressure effects on the optical-absorption edge of CdIn₂S₄, MgIn₂S₄, MnIn₂S₄ thiospinels. *J. Appl. Phys.* **103**, 063710 (2018)
- E. Lefterova, P. Angelov, V. Ilcheva, T. Petkova, Y. Dimitriev, in *Investigation of AgI–Ag₂SO₄–TeO₂ Glasses and Glass Ceramics*. ed. by E. Balabanova, I. Dragieva. Nanoscience & Nanotechnology, vol. 4 (Heron Press, Sofia, 2004)
- S. Rada, M. Culea, E. Culea, Structure of TeO₂ B₂O₃ glasses inferred from infrared spectroscopy and DFT calculations. *J. Non-Cryst. Solids* **354**, 5491–5495 (2008)
- G. Meunier, R. Dormoy, A. Levasseur, New positive-electrode materials for lithium thin film secondary batteries. *Mater. Sci. Eng. B* **3**, 19 (1989)
- M. Natarajan, C.N.R. Rao, Phase transitions in silver halides: silver iodide and its solid solutions with silver bromide. *J. Chem. Soc. A*, 3087–3092 (1970)
- V. Kozhukharov, S. Nikolav, M. Marinov, T. Troev, Studies of glass structure in the TeO₂–Fe₂O₃ system. *Mater. Res. Bull.* **14**, 735 (1979)
- M. Arnaudov, V. Dimitrov, Y. Dimitriev, L. Markova, Infrared-spectral investigation of tellurites. *Mater. Res. Bull.* **17**, 1121 (1982)
- S. Rada, E. Culea, V. Rus, M. Pica, M. Culea, The local structure of gadolinium vanado-tellurite glasses. *J. Mater. Sci.* **43**, 3713
- A. Levasseur, J.C. Brethous, J.M. Reau, P. Hangenmuller, M. Couzi, Synthesis and characterization of new solid electrolyte conductors of lithium ions. *Solid State Ion.* **1**, 177–186 (1980)
- W.L. Konijnendijk, J.M. Stevels, The structure of borate glasses studied by Raman scattering. *J. Non-Cryst. Solids* **18**, 307 (1975)
- F. Yakuphanoglu, A. Cukurovalib, I. Yilmaz, Determination and analysis of the dispersive optical constants of some organic thin films. *Physica B* **351**, 53–58 (2004)
- M. Caglar, S. Ilican, Y. Caglar, Y. Sahin, F. Yakuphanoglu, D. Hur, A spectroelectrochemical study on single-oscillator model and optical constants of sulfonated polyaniline film. *Spectrochim. Acta Part A* **71**, 621–627 (2008)
- F. Urbach, The long-wavelength edge of photographic sensitivity and of the electronic absorption of solids. *Phys. Rev.* **92**, 1324 (1953)
- V. Dimitrov, S. Sakka, Electronic oxide polarizability and optical basicity of simple oxides. *J. Appl. Phys.* **79**, 1736 (1996). <https://doi.org/10.1063/1.360962>
- R. Parmar, R.S. Kundu, R. Punia, N. Kishore, P. Aghamkar, Fe₂O₃ modified physical, structural and optical properties of bismuth silicate glasses. *J. Mater.* **2013**, 5. Article ID 650207 (2013).
- B. Sujatha, C. Narayana Reddy, R.P.S. Chakradhar, Dielectric relaxation and ion transport in silver–boro-tellurite glasses. *Philos. Mag.* **90**(19), 2635–2650 (2010)
- S. Kalyanaramana, P.M. Shajinshinuab, S. Vijayalakshmi, J. Phys. Chem. Solids **86**, 108–113 (2015)

26. F.A. Miranda, F.W. Vankeuls, R.R. Romanofsky, C.H. Mueller, S. Alterovitz, G. Subramanyam, *Integr. Ferroelectr.* **42**, 131 (2002)
27. R.H. Al Orainy, Single oscillator model and refractive index dispersion properties of ternary ZnO films by sol gel method. *J. Sol-Gel Sci. Technol.* (2014). <https://doi.org/10.1007/s10971-014-3272-1>
28. E.M. Masoud, M. Khairy, M.A. Mousa, *J. Alloys Compd.* **569**, 150–155 (2013)

Publisher's Note Springer Nature remains neutral with regard to jurisdictional claims in published maps and institutional affiliations.